The Island Arc (2001) **10**, 98–115

Research Article

Cooling and inferred exhumation history of the Ryoke metamorphic belt in the Yanai district, south-west Japan: Constraints from Rb–Sr and fission-track ages of gneissose granitoid and numerical modeling

TAKAMOTO OKUDAIRA,[1,*] YASUTAKA HAYASAKA,[2] OSAMU HIMENO,[3] KOICHIRO WATANABE,[3] YASUHIRO SAKURAI[4] AND YUKIKO OHTOMO[5]

[1]*Department of Geosciences, Osaka City University, Osaka 558-8585, Japan, (email: oku@sci.osaka-cu.ac.jp)* [2]*Department of Earth and Planetary Systems Science, Hiroshima University, Higashi-Hiroshima 739-0046, Japan,* [3]*Department of Earth Resource Engineering, Kyushu University, Fukuoka 812-8581, Japan,* [4]*Ikeshinden High School, Hamaoka 437-1612, Japan and* [5]*Department of Sciences, Yamagata University, Yamagata 990-0021, Japan*

Abstract The Ryoke metamorphic belt in south-west Japan consists mainly of I-type granitoids and associated low-pressure/high-temperature metamorphic rocks. In the Yanai district, it has been divided into three structural units: northern, central and southern units. In this study, we measured the Rb–Sr whole-rock–mineral isochron ages and fission-track ages of the gneissose granodiorite in the central structural unit. Four Rb–Sr ages fall in a range of *ca* 89–87 Ma. The fission-track ages of zircon and apatite are 68.9 ± 2.6 Ma and 57.4 ± 2.5 Ma (1σ error), respectively. Combining the newly obtained ages with previously reported (Th–)U–Pb ages from the same unit, thermochronologic study revealed two distinctive cooling stages; 1) a rapid cooling (> 40°C/Myr) for a period (~7 Myr) soon after the peak metamorphism (~ 95 Ma) and 2) the subsequent slow cooling stage (~ 5°C/Myr) after *ca* 88 Ma. The first rapid cooling stage corresponds to thermal relaxation of the intruded granodiorite magma and its associated metamorphic rocks, and to the uplift by a displacement along low-angle faults which initiated soon after the intrusion of the magma. Uplift by the later stage deformation having formed large-scale upright folds resulted in progress of the exhumation during the first stage. The average exhumation velocity of the stage is ≥ 2 mm/yr. During the second stage, the rocks were not accompanied by ductile deformation and were exhumed with the rate of 0.1–0.2 mm/yr. The difference in the exhumation velocity between the first and second cooling stages resulted from the difference in the thickness of the crust and in the activity of ductile deformation between the early and later stages of the orogenesis.

Key words: Arc–trench system, cooling history, exhumation, fission-track age, Rb–Sr isochron age, Ryoke metamorphic belt, south-west Japan.

INTRODUCTION

The Ryoke metamorphic belt in south-west Japan is known to be a Cretaceous low-pressure type regional metamorphic belt. It consists mainly of a large volume of I-type granitoids and associated low-pressure/high-temperature metamorphic rocks. The Ryoke metamorphic belt, together with the high-pressure Sambagawa metamorphic belt, is a typical example of paired metamorphic belts in the Circum-Pacific regions (e.g. Miyashiro 1994; Nakajima 1994). It is considered that the Ryoke metamorphic belt formed beneath a volcanic arc or forearc at a depth of 10–20 km and the Sambagawa metamorphic belt developed near a trench zone at ~ 30 km deep (e.g. Miyashiro 1994). They have been juxtaposed by the Median Tectonic Line (MTL) during Late Cretaceous (e.g. Ohtomo 1993;

*Correspondence. Received 4 February 2000; accepted for publication 29 September 2000.

Brown 1998). Such a paired metamorphic belt is a key to understanding the evolutionary processes of the continental crust in an arc–trench system.

The Ryoke granitoids have been classified into two groups, Older and Younger granitoids, based on their field relations and lithological characteristics (e.g. Ryoke Research Group 1972; Kutsukake 1993). The Older granitoids intrude concordantly into the high-grade metamorphic rocks without the development of contact aureoles. In contrast, the Younger granitoids intrude discordantly into the low- to medium-grade metamorphic rocks and are accompanied by the formation of contact aureoles. The Older and Younger granitoids are of sheet- and stock-like intrusions, respectively (e.g. Hara *et al.* 1991). Systematic age progression from Older to Younger granitoids is evidenced by the monazite ages for the U–Th–Pb systematics (CHIME) of Suzuki and Adachi (1998), and then this classification has been supported.

Thermochronological analysis, based on the relationship between radiometric ages and closure temperatures determined for different radiogenic isotope systems, provides information for the uplift and/or exhumation processes of the deep-seated plutono-metamorphic complex (e.g. McDougall & Harrison 1988; Spear 1993). Recently, detailed thermochronological analyses have been performed on the Ryoke metamorphic belt (e.g. Tagami *et al.* 1988; Yuhara & Kagami 1995; Suzuki & Adachi 1998). In the present study, to clarify the cooling history of the Ryoke metamorphic belt in the Yanai district, Rb–Sr and fission-track ages of the Older granitoids are reported. The cooling and inferred exhumation history of the rocks will also be discussed, based on the thermochronological analysis and numerical modeling.

GEOLOGICAL REMARKS

In the Yanai district, the Ryoke metamorphic belt consists mainly of the Older granitoids (Gamano granodiorite and Tengatake-Nagano migmatite), the Younger granitoid (Kibe granite) and the low-pressure metamorphic rocks (e.g. Higashimoto *et al.* 1983; Okudaira *et al.* 1993; Fig. 1). The Gamano granodiorite is the most widely occurring Older granitoid in the district. It is mainly composed of hornblende–biotite tonalite and hornblende-bearing biotite granodiorite. In the northern part of Yashirojima Is. the well-foliated granodiorite develops and has been considered to be a fragment of the pre-Ryoke basement rocks to the Upper Paleozoic geosyncline of south-west Japan (Kojima & Okamura 1968). However, because there are geochemical and geochronological similarities between the well-foliated granodiorite and the Gamano granodiorite, the two are correlated as part of the same body (Honma & Sakai 1975; Shigeno & Yamaguchi 1976; Sakurai & Hara 1990; Suzuki *et al.* 1994; Okudaira 1996b; Herzig *et al.* 1998; Suzuki & Adachi 1998).

The metamorphic rocks are derived from the Jurassic accretionary complex (Kuga Group: cf. Higashimoto *et al.* 1983). They are divided into several mineral zones based on mineral paragageneses of metapelites and metapsammites, as biotite, cordierite, sillimanite and garnet–cordierite zones (e.g. Ikeda 1991; Okudaira *et al.* 1993; Nakajima 1994). Herein we follow the mineral zones defined by Okudaira *et al.* (1993). The garnet zone of Okudaira *et al.* (1993) is renamed here as the garnet–cordierite zone, because it is more informative about the index mineral assemblage. Each mineral zone is characterized by the following mineral assemblages: biotite zone (biotite + muscovite), cordierite zone (cordierite + K-feldspar + biotite + muscovite + andalusite), sillimanite zone (sillimanite + K-feldspar + biotite + cordierite or garnet), and garnet–cordierite zone (garnet + cordierite + K-feldspar + biotite). According to the pressure–temperature estimates by Okudaira (1996b), the metamorphic conditions of these zones are: 460–590°C at ~300 MPa (cordierite zone), 630–690°C at 300–500 MPa (sillimanite zone), and 730–770°C at 550–650 MPa (garnet–cordierite zone). Inferred metamorphic field gradient of the metamorphic belt is of 40–50°C km^{-1}. The high-grade mineralogy of low-pressure Ryoke metamorphism results from the thermal effects by intrusion of the Gamano granodiorite (Okudaira *et al.* 1993; Okudaira 1996a,b,c; Ikeda 1998a,b).

As shown in Fig. 2, structural evolution of the district has been summarized as (i) intrusion of the Older granitoid magma along the low-angle normal faults dipping to the north (D1), followed by low-pressure type metamorphism, and (ii) formation of low-angle thrusts and faults dipping to the north and of large-scale recumbent folds and nappes (D2), and upright folding with east-west trending axes (D3). It is considered that D1 deformation event occurred in an arc-normal extensional stress field, whereas D2 and D3 deformation events took place under arc-normal compression

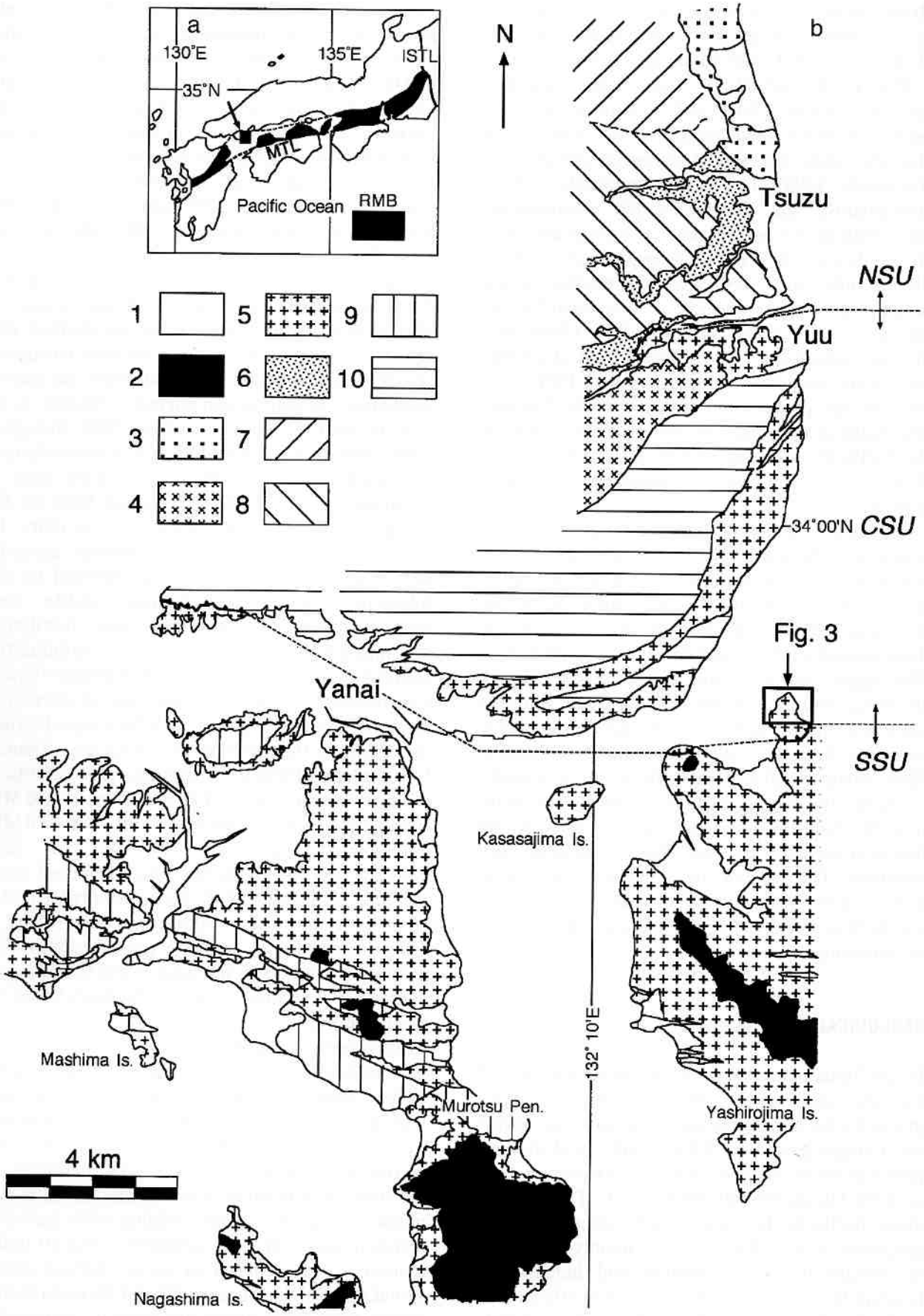
a
130°E
135°E
ISTL
35°N
MTL
Pacific Ocean
RMB
1
2
3
4
5
6
7
8
9
10
N
b
Tsuzu
NSU
Yuu
34°00'N
CSU
Fig. 3
Yanai
SSU
Kasasajima Is.
Mashima Is.
Murotsu Pen.
132° 10'E
Yashirojima Is.
4 km
Nagashima Is.

Fig. 1 (a) Outline map showing the location of the Ryoke metamorphic belt of south-west Japan. RMB, Ryoke metamorphic belt; MTL, Median Tectonic Line; ISTL, Itoigawa–Shizuoka Tectonic Line. (b) Geological and metamorphic zonation map of the Yanai district. 1, alluvium; 2, Tertiary volcanics; 3, Iwakuni granite; 4, Younger Ryoke granitoid (Kibe granite); 5 and 6, Older Ryoke granitoids (5 Gamano granodiorite, 6 Tengatake–Nagano migmatite); 7–10, Ryoke metamorphic rocks (7 biotite zone, 8 cordierite zone, 9 sillimanite zone, 10 garnet–cordierite zone). NSU, Northern structural unit; CSU, Central structural unit; SSU, Southern structural unit.

and arc–parallel extension stress regime (Okudaira 1996b,c). The intrusion of the Younger granitoids post-dated the formation of the D3-upright folds. During and after D1, the Older granitoids and metamorphic rocks experienced the same deformational history, therefore their cooling and exhumation histories are mostly comparable. The D2 deformation event formed a pile nappe structure consisting of three structural units, such as northern, central and southern units (Okudaira *et al.* 1993; Okudaira 1996b,c). These structural units are separated by low-angle normal and thrust faults.

RUBIDIUM–STRONTIUM AND FISSION-TRACK DATING

SAMPLE DESCRIPTION

Analyzed samples were collected from the Hirarehana Peninsula, northern part of Yashirojima Is. The samples belong to the central structural unit. Localities of the samples are plotted on the route map of Kojima and Okamura (1968) as illustrated in Fig. 3.

Sample OG-1 has a distinct gneissose structure and is of granodiorite–tonalite modal composition. Biotite clot is a characteristic structure. Sakurai and Hara (1990) named the rock coarse-grained layer. It consists mainly of plagioclase, quartz, biotite and small amounts of interstitial K-feldspar. Accessory minerals are zircon, apatite, ilmenite, allanite and monazaite. Plagioclase is distinctly zoned (core An_{83}, rim An_{33}). Where plagioclase is in contact with K-feldspar (Or_{89}), myrmekitic plagioclase (An_{42-20}) develops (Sakurai & Hara 1988, 1990; T. Okudaira, unpubl. data, 1992). Although the long axes of euhedral plagioclase and biotite grains are preferentially oriented parallel to the lithological boundaries, solid-state deformation structures, such as undulatory extinction of quartz grains and deformation twin of plagioclase grains are not common, suggesting that solid-state deformation was not well-developed.

Sample OG-2 is a leucocratic granite vein intruding parallel to the coarse-grained layers (OG-1). It is composed of quartz and subhedral plagioclase, with subordinate amounts of biotite and interstitial K-feldspar. Plagioclase and K-feldspar compositions are An_{40-35} and Or_{84}, respectively (Sakurai & Hara 1990).

Samples OG-3 and OG-10 are fine-grained gneissose tonalite. They are composed of quartz, plagioclase and biotite. Zircon, apatite, ilmenite, allanite and monazite are accessory minerals. The (010) planes of plagioclase are intensely aligned parallel to the foliation defined by preferred shape orientation of biotite aggregates, whereas quartz *c*-axes are randomly distributed. Solid-state deformation structures are rarely observed, whereas the long axes of subhedral plagioclase and biotite grains are strongly aligned parallel to the foliation.

Samples OG-4, 5, 6, and 7 are sheets and blocks of diorite included in the granitic rocks. These diorites consist of plagioclase, hornblende and rarely clinopyroxene or quartz. Accessory minerals are apatite, ilmenite and zircon. Coarse-grained diorites (OG-4 and -6) show a distinct foliation marked by an alignment of euhedral plagioclase crystals, but fine-grained ones (OG-5 and -7) show random fabric of subhedral plagioclase grains.

Samples OG-8 U, OG-8 L, OG-9, and OG-11 are gneissose granodiorite–adamellite. These granitic rocks contain porphyritic K-feldspar (up to 4 cm) and are distinguishable from those of the coarse-grained layer by the modal amount of K-feldspar in the quartz–alkali-feldspar–plagioclase ternary diagram. Zircon, apatite, ilmenite, allanite and monazite grains can be identified as accessory minerals. The K-feldspar contains inclusions of fine-grained plagioclase, quartz, biotite and shows perthite structure. Where plagioclase is in contact with K-feldspar, myrmekite is well-developed.

ANALYTICAL METHODS

Measurement of Rb–Sr isotopic ratios followed the method of Kagami *et al.* (1987, 1989) and was performed by using MAT 261 mass spectrometer (Finningan Mat, San Jose, USA) at the Institute

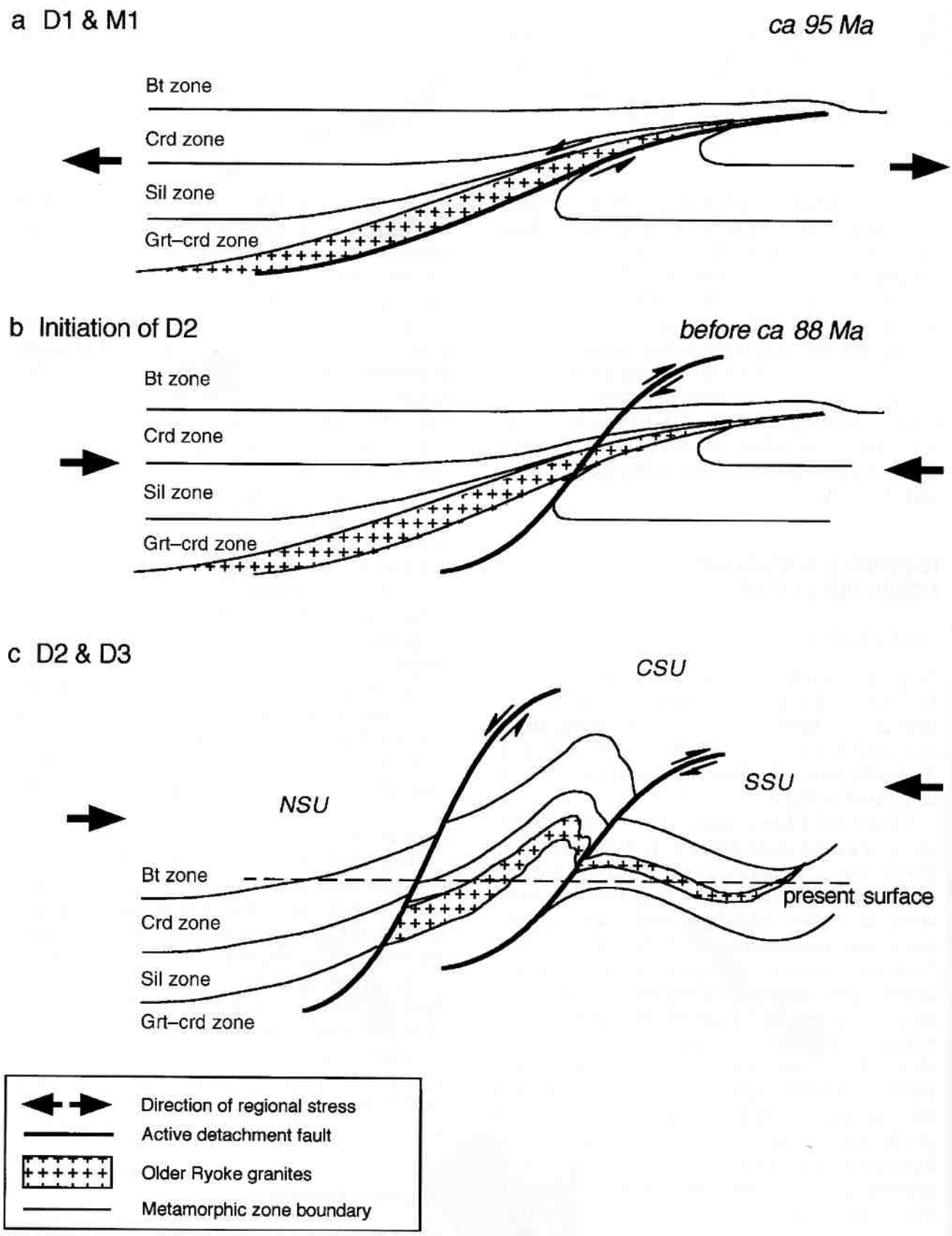

Fig. 2 A possible tectonic model for the Ryoke metamorphic belt during Late Cretaceous period (after Okudaira 1996c). NSU, Northern structural unit; CSU, Central structural unit; SSU, Southern structural unit; bt, biotite zone; crd, cordierite zone; sil, sillimanite zone; grt–crd, garnet–cordierite zone.

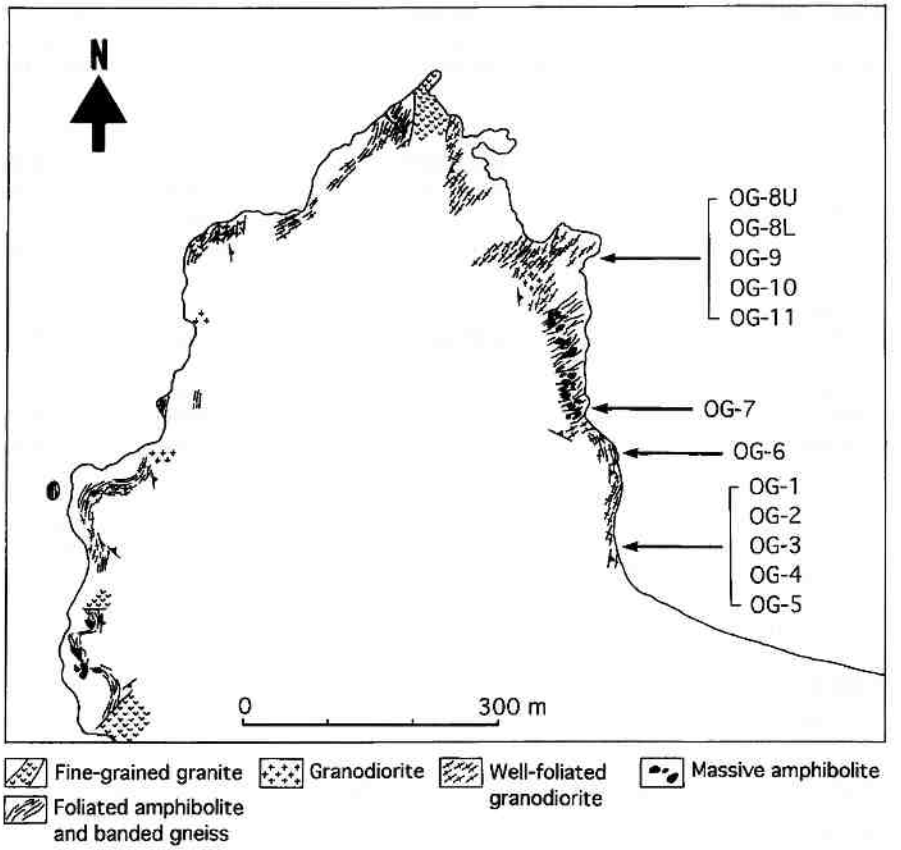

Fig. 3 Sample localities shown on the route map modified partly from Kojima and Okamura (1968), Hirarehana, Yashirojima island.

for Studies of Earth's Interior, Okayama University. The measured $^{87}Sr/^{86}Sr$ ratios are normalized to $^{88}Sr/^{86}Sr = 8.375\,209$. $^{87}Sr/^{86}Sr$ ratio of the standard NBS987 is $0.710\,248 \pm 0.000\,007$ during the measurement. Decay constant of $\lambda^{87}Rb$ is 1.42×10^{-11}/yr (Steiger & Jäger 1977). The Rb and Sr concentrations were determined by the isotope dilution method. To calculate Rb–Sr isochron age, errors of 0.5% and 0.01% were assumed for the isotope dilution method and for $^{87}Sr/^{86}Sr$, respectively. Rb–Sr isochron ages and initial Sr isotope ratios (SrI) were calculated using a program of Kawano (1994) utilizing the equation of York (1966).

Fission-track (FT) dating was carried out for the sample OG-1. Grains of zircon and apatite were mounted in PFA Sheet (Toray, Tokyo, Japan) and Araldite (Vantico, Basel, Switzerland) resin, respectively and polished to expose the grain surface. Zircon samples were etched for 19 h in NaOH + KOH eutectic at 230°C to reveal the fossil FT. Apatite samples were etched for 25 s in 5M HNO_3 at 24°C. Both zircon and apatite mounts were processed using the external detector method (e.g. Gleadow 1981). Thermal neutron irradiation was carried out by TRIGA MARK II reactor (General Atomics, San Diego, USA) in Rikkyo University for the zircon mount package and also by a Slowpoke reactor (AECL, Ontario, Canada) in Dalhousie University for apatite. Reported cadmium ratio for Au in each reactor is about 3 and 4.2, respectively. Mica detectors on zircon mounts and standard glasses included in zircon irradiation packages were etched in 48% hydrogen fluoride (HF) at 25°C for 10 min and 20 min, respectively. Micas on apatite mounts and on standard glasses were etched at 23°C for 20 min and 27 min. Ages were determined using the zeta calibration method (Hurford & Green 1983). Zeta values were obtained for the age standard of Fish Canyon Tuff (FCT) zircon and apatite, Buluk Member Tuff (BMT) zircon and Durango apatite (Table 1).

RESULTS

The concentrations of Rb, Sr and isotopic ratios of $^{87}Rb/^{86}Sr$ and $^{87}Sr/^{86}Sr$ are listed in Table 2. The $^{87}Rb/^{86}Sr$ versus $^{87}Sr/^{86}Sr$ plots of all whole-rock

Table 1 Zeta values were obtained for the age standard of FCT zircon and apatite, BMT zircon and Durango apatite

Sample code	No. grains	Spontaneous ρs (Ns) $\times 10^5$/cm^2	Induced ρi (Ni) $\times 10^5$/cm^2	Dosimeter ρd (Nd) $\times 10^6$/cm^2	P(χ^2) %	Zeta ±1σ
Zircon						
FCT1	30	55.2 (1229)	57.1 (1271)	1.45 (2059)	58	398±18
FCT2	30	56.8 (1537)	57.9 (1568)	1.45 (2059)	11	393±17
BMT1	28	10.7 (269)	17.5 (442)	1.45 (2059)	63	373±30
BMT2	40	8.91 (332)	15.6 (580)	1.45 (2059)	72	397±29
					Weighted mean zeta:	393±11
Apatite						
FCT1	30	2.20 (209)	11.7 (1113)	10.0 (4704)	95	296±23
FCT2	30	2.05 (136)	11.6 (769)	10.1 (4704)	95	314±30
FCT3	30	1.92 (173)	10.2 (919)	10.1 (4704)	79	294±24
Durango 1	1	1.46 (543)	7.51 (2796)	10.1 (4704)	43	322±17
Durango 2	1	1.52 (565)	8.17 (3044)	10.1 (4704)	98	336±17
					Weighted mean zeta:	318±9

Note: ρ and N denote track density and number of tracks counted, respectively. Analysis was made by the external detector method using geometry factor of 0.5 and zeta values were determined for dosimeter glass SRM612. P(χ^2) is Chi square probability (Green 1981). FCT, Fish Canyon Tuff; BMT, Buluk Member Tuff.

Table 2 Analytical results of isotopes of Rb-Sr system for the rocks located in the Hirarehana Peninsula

Sample	Lithology	Rb (p.p.m.)	Sr (p.p.m.)	$^{87}Rb/^{86}Sr$	$^{87}Sr/^{86}Sr$*
OG-1	Granodiorite	69.3	336	0.5970	0.709547
	Biotite	420	22.4	54.66	0.776449
OG-2	Granitic vein	14.1	282	0.1449	0.708809
OG-3	Tonalite	105	275	1.106	0.709830
OG-4	Diorite	52.6	387	0.3934	0.708643
OG-5	Diorite	47.8	313	0.4420	0.708451
OG-6	Diorite	42.5	450	0.2734	0.708297
OG-7	Diorite	47.7	340	0.4056	0.708299
OG-8 U	Granodiorite	87.3	293	0.8632	0.708788
	Plagioclase	10.2	440	0.0672	0.707778
	K-feldspar	203	482	1.220	0.709286
	Biotite	177	34.2	14.98	0.726339
OG-8 L	Granodiorite	85.6	307	0.8058	0.708727
	Plagioclase	6.33	516	0.0355	0.707750
	K-feldspar	188	544	0.9982	0.708990
	Biotite	243	12.2	57.80	0.781091
OG-9	Adamellite	78.8	287	0.7938	0.708820
OG-10	Tonalite	74.3	304	0.7060	0.708722
OG-11	Adamellite	83.9	279	0.8700	0.708988
	Plagioclase	8.23	551	0.0432	0.707964
	K-feldspar	207	423	1.416	0.709744
	Biotite	398	5.45	216.6	0.978459

*$^{87}Sr/^{86}Sr$ ratios were normalized to $^{88}Sr/^{86}Sr = 8.375209$.

samples are shown in Fig. 4. They are scattered and do not yield an isochron. As shown in Fig. 5, an isochron using the whole-rock and biotite of sample OG-1 yields 87.1±0.5 Ma (SrI = 0.708 808± 0.000 007). Isochrons for whole-rock, plagioclase, K-feldspar and biotite of samples OG-8 U, OG-8 L and OG-11 give 87.5±0.7 Ma (SrI = 0.707 725 ±0.000 047), 89.4±0.1 Ma (SrI = 0.707 710± 0.000 012) and 87.9±0.5 Ma (SrI = 0.707 928± 0.000 046), respectively. The Rb–Sr ages range from 87 to 89 Ma (Fig. 5), which are comparable to the Rb–Sr whole-rock-biotite isochron age (89.4 ±4.0 Ma recalculated based on $\lambda^{87}Rb = 1.42 \times 10^{-11}$/yr) of Shigeno and Yamaguchi (1976). The SrI ratios measured here range from 0.707 710 to 0.708 808, which are slightly higher than those of

Table 3 Results of Fission-track dating for zircon and apatite grains from the Gamano granodiorite (sample OG-1)

Sample code	No. grains	Spontaneous ρs (Ns)	Induced ρi (Ni)	Dosimeter ρd (Nd)	$P(\chi^2)$ %	Age ± error Ma 1 σ
Zircon		$\times 10^6/cm^2$	$\times 10^6/cm^2$	$\times 10^5/cm^2$		
Sheet 1	19	10.0 (1098)	3.82 (419)	1.45 (2059)	46	74.3 ± 5.0
Sheet 2	16	9.47 (953)	4.14 (417)	1.45 (2059)	37	64.8 ± 4.4
Sheet 3	17	10.7 (1233)	4.48 (516)	1.45 (2059)	41	67.7 ± 4.3
					Weighted mean:	68.9 ± 2.6
Apatite		$\times 10^5/cm^2$	$\times 10^6/cm^2$	$\times 10^6/cm^2$		
Sheet 1	18	7.98 (231)	2.30 (667)	1.02 (4704)	60	55.7 ± 4.6
Sheet 2	17	8.41 (389)	2.25 (1043)	1.02 (4704)	95	60.0 ± 4.1
Sheet 3	15	8.49 (302)	2.46 (874)	1.02 (4704)	16	55.7 ± 4.1
					Weighted mean:	57.4 ± 2.5

Note: ρ and N denote track density and number of tracks counted, respectively. Analysis was made by the external detector method using geometry factor of 0.5. Ages were calculated using zeta values of 393 and 318 for zircon and apatite, respectively, determined for dosimeter glass SRM612. $P(\chi^2)$ is Chi square probability (Green 1981).

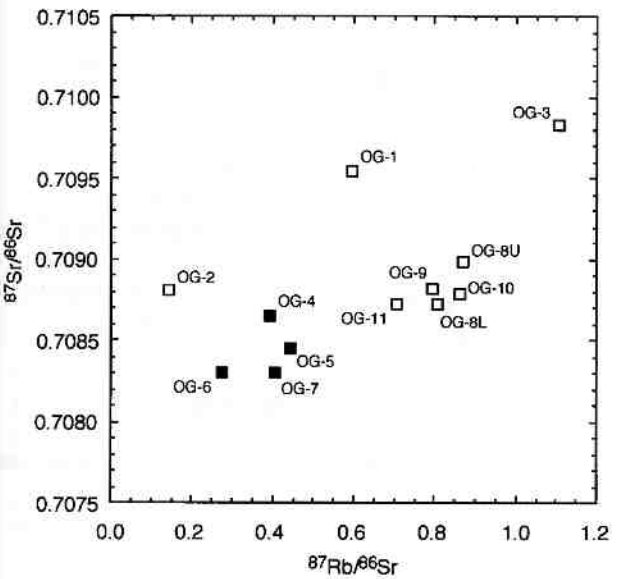

Fig. 4 $^{87}Rb/^{86}Sr$ *vs* $^{87}Sr/^{86}Sr$ diagram for all whole-rock samples. (□), granitoid; (■), diorite.

the Gamano granodiorite analyzed by Shigeno and Yamaguchi (1976) and Okano and Honma (1983), that is, 0.7073–0.7077.

The track count data for zircon and apatite FT age determinations are shown in Table 3. The zircon and apatite grains yield 68.9 ± 2.6 Ma and 57.4 ± 2.5 Ma (1 σ error), respectively. Three mount sheets were prepared for each of the zircon and apatite samples to see the fluctuation of the whole analytical procedures and weighted mean FT ages were obtained to represent the results. The FT ages are shown as pooled ages with conventional errors (Green 1981). All $P(\chi^2)$ values exceed 5% and support the assumption that all dated grains belong to a single age population and single grain ages vary in a range of random generation of FT (Galbraith 1981).

Chlorine to fluorine ratio of apatite strongly affects annealing behavior of the FT (Green *et al.* 1986; O'Sullivan & Parrish 1995). Fission-tracks in Cl-rich apatite are more resistant to track annealing and thus the closure temperature for Cl-rich apatite is significantly higher than widely accepted closure temperature (110°C). Chlorine contents of apatite were determined for 18 dated grains of the mount sheet 1. Microprobe analysis was carried out at Dalhousie University using SP-733 (JEOL, Tokyo, Japan) with operating parameters of 15 kV acceleration voltage, 15 nA current and 10 μm beam size. Chlorine content of each grain is plotted against apatite single grain FT age in Fig. 6. Apatite grains were found to be dominantly fluorine apatite and the chlorine contents of each grain ranged from 0 to 0.2 wt%. Systematic variation of age with chlorine content is not identified.

DISCUSSION

THERMOCHRONOLOGICAL ANALYSIS

The samples analyzed here belong to the central structural unit. To clarify thermochronological feature of the central unit, radiometric ages of the rocks in the unit published to date are compiled along with our results (Table 4). Ages of the Younger Ryoke granitoids are omitted in this compilation, because thermal (cooling) history of the

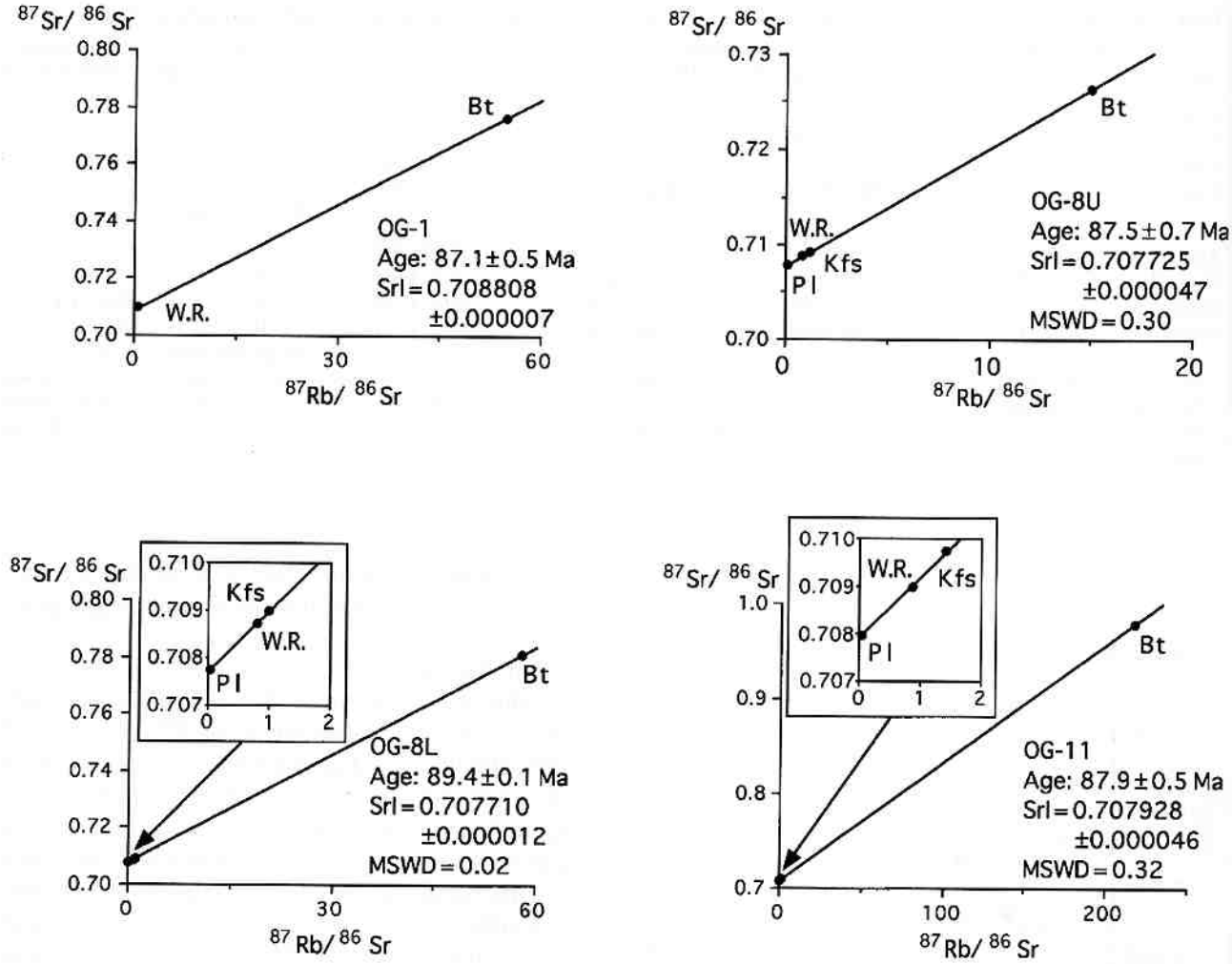

Fig. 5 Rb–Sr whole-rock–mineral isochron for the samples. Isochron ages, initial Sr ratios (SrI) and mean squares of weighted deviates (MSWD) are shown in the figures. W.R., whole rock; Pl, plagioclase; Kfs, K-feldspar; Bt, biotite.

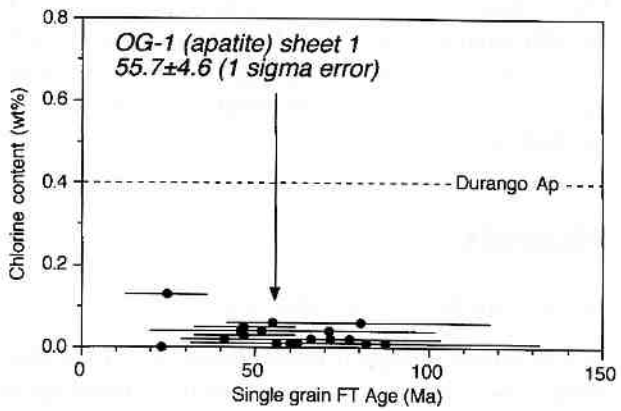

Fig. 6 Weighted-percent of chlorine plotted against the apatite single grain ages for each of 18 dated grains from sample OG-1 (sheet 1).

Younger granitoids is distinct from that of the Older granitoids and metamorphic rocks (e.g. Hara *et al.* 1991; Okudaira *et al.* 1993). In this thermochronological analysis, thermal effect of the intrusion of the Younger granitoids is negligible, because the contact aureoles developed around the Younger granitoids are restricted to ≤2 km width (Higashimoto *et al.* 1983; Nureki *et al.* 1992). The granodiorite samples are about 5 km away from the nearest Younger granitoid (Towa granite: Kojima & Okamura 1968).

In this study, the following closure temperatures are adopted: U–Pb zircon is 750±50°C, Th–U–Pb monazite (CHIME) is 700±50°C, K–Ar biotite is 270±40°C and Rb–Sr biotite is 310±40°C (Jäger 1979; Hurford 1986; McDougall & Harrison 1988; Spear 1993; Suzuki *et al.* 1994). As the whole-rock—mineral isochron ages studied here largely

Table 4 Summary of geochronological data in the central structural unit of the Ryoke metamorphic belt of the Yanai district

Sample	Method	Age (Ma)	Reference
Granodiorite	Rb–Sr (W.R.–Bt)	89.4±4.0*	1
	Rb–Sr (W.R.–Bt)	87.1±0.5	This study
	Rb–Sr (W.R.–Bt)	87.5±0.7	This study
	Rb–Sr (W.R.–Bt)	89.4±0.1	This study
	Rb–Sr (W.R.–Bt)	87.9±0.5	This study
	K-Ar (Bt)	89.5±4.5	2
	SHRIMP (Zrn)	101.0±1.9	3
	CHIME (Mnz)	95.2±3.9	4
	CHIME (Mnz)	95.1±6.4	6
	U–Pb (Zrn)	96.2±3.0	7
	U–Pb (Zrn)	95.3±1.0	7
	FT (Zrn)	68.9±2.6 (1σ)	This study
	FT (Ap)	57.4±2.5 (1σ)	This study
Metapelite	CHIME (Mnz)	98.8±3.3	4
	CHIME (Mnz)	98.4±4.2	4
	CHIME (Mnz)	98.9±2.1	5
	CHIME (Mnz)	99.6±2.4	5
	CHIME (Mnz)	99.6±2.4	5
	CHIME (Mnz)	100.7±3.2	6
	CHIME (Mnz)	100.5±3.0	6
	CHIME (Mnz)	100.5±3.1	6

*Recalculated by decay constant of λ^{87}Rb to be 1.42×10^{-11}/yr. FT, fission-track; W.R., whole rock; Bt, biotite; Zrn, zircon; Mnz, monazite; Ap, apatite; CHIME, chemical Th–U-total Pb isochron method.

References: 1. Shigeno and Yamaguchi (1976), 2. Higashimoto *et al.* (1983), 3. Nakajima *et al.* (1993), 4. Suzuki *et al.* (1994), 5. Suzuki *et al.* (1996), 6. Suzuki and Adachi (1998), 7. Herzig *et al.* (1998).

depend on the isotope ratio of biotite, closure temperatures of the isochron ages are controlled by that of biotite for Rb–Sr system (i.e. 310±40°C). For fission-track dating, the closure temperatures of zircon and apatite are 240±50°C (Hurford 1986; Tagami *et al.* 1999) and 110±15°C (Nishimura & Mogi 1986), respectively.

In contrast, the CHIME monazite ages of metapelites do not represent the cooling age for the closure temperature (700±50°C) during retrograde stage, but indicate the timing of crystallization of metamorphic monazite at 525±25°C during prograde stage (Smith & Barreiro 1990; Suzuki *et al.* 1994). Although the peak temperatures of the metapelites in the central structural unit are of 730–770°C (Okudaira 1996b), the period of the peak metamorphism was probably too short to reset the ages and then the peak metamorphism was younger than 101–98 Ma (Suzuki *et al.* 1994). The CHIME monazite ages and U–Pb zircon ages of the Older granitoids concentrate in a range of 96–95 Ma (Table 4), except for the data of Nakajima *et al.* (1993) which is older than other ages by approximately 5 Ma. The Ryoke metamorphism was caused by thermal effect of the intrusion of the Older granitoids (Okudaira 1996a,b; Ikeda 1998a,b), and then the ages of the peak metamorphism can be considered to be closed to the crystallization age of the Older granitoids. Consequently, the age of the crystallization of the granodiorite and the peak metamorphism was approximately 95 Ma.

The ages of the Gamano granodiorites and metapelites by different systems along with the closure or crystallization temperatures are shown in Fig. 7. From approximately 750–300°C, cooling rate of the unit was rapid (>40°C/Myr) until ~90 Ma. Following the rapid cooling stage, temperature decreased from approximately 300–100°C very slowly (~5°C/Myr). The rapid and slow cooling stages are hereafter called the first and second cooling stages, respectively. Rb–Sr mineral isochron ages of the granitoids concentrate in a range of 89–87 Ma. Difference between Rb–Sr biotite and fission-track zircon ages is relatively large (~20 Myr), although difference between their closure temperatures is small (approximately 70°C). Therefore, 7 million years is a maximum estimation for the period of the first cooling stage from 750 to 310°C.

TECTONIC IMPLICATION

Tectonics related to the first cooling stage

Depth of intrusion of the Gamano granodiorite magma was ~15–20 km, based on the pressure estimates of the overlying sillimanite zone, P= 0.3–0.5 GPa, and the underlying garnet-cordierite zone, P=0.55–0.65 GPa (Okudaira 1996b). This estimation is more or less supported by calculated crystallization pressure of the Gamano granodiorite (0.43±0.06 GPa: average Al content of hornblende=1.54 per formula unit), using the Al-in-hornblende geobarometer of Schmidt (1992). If the granodiorite magma intruded at that depth and did not exhume, it cooled until ~600°C, which is the temperature of the rocks at a middle crustal level (approximately 20 km) with a geothermal gradient of 30°C/km assumed. The geothermal gradient of 30°C/km is the mean value for an active continental margin or island arc (Sugimura & Uyeda 1973). As the first rapid cooling stage continued at least until 300°C, it is necessary that the granodiorite should have exhumed or came in contact with a cooler geologic unit or fluid for its temperature to decrease furthermore (Peacock 1991; Spear 1993). From the point of view of exhumation, to cool the rocks to 300°C, exhumation of the central structural unit must have begun

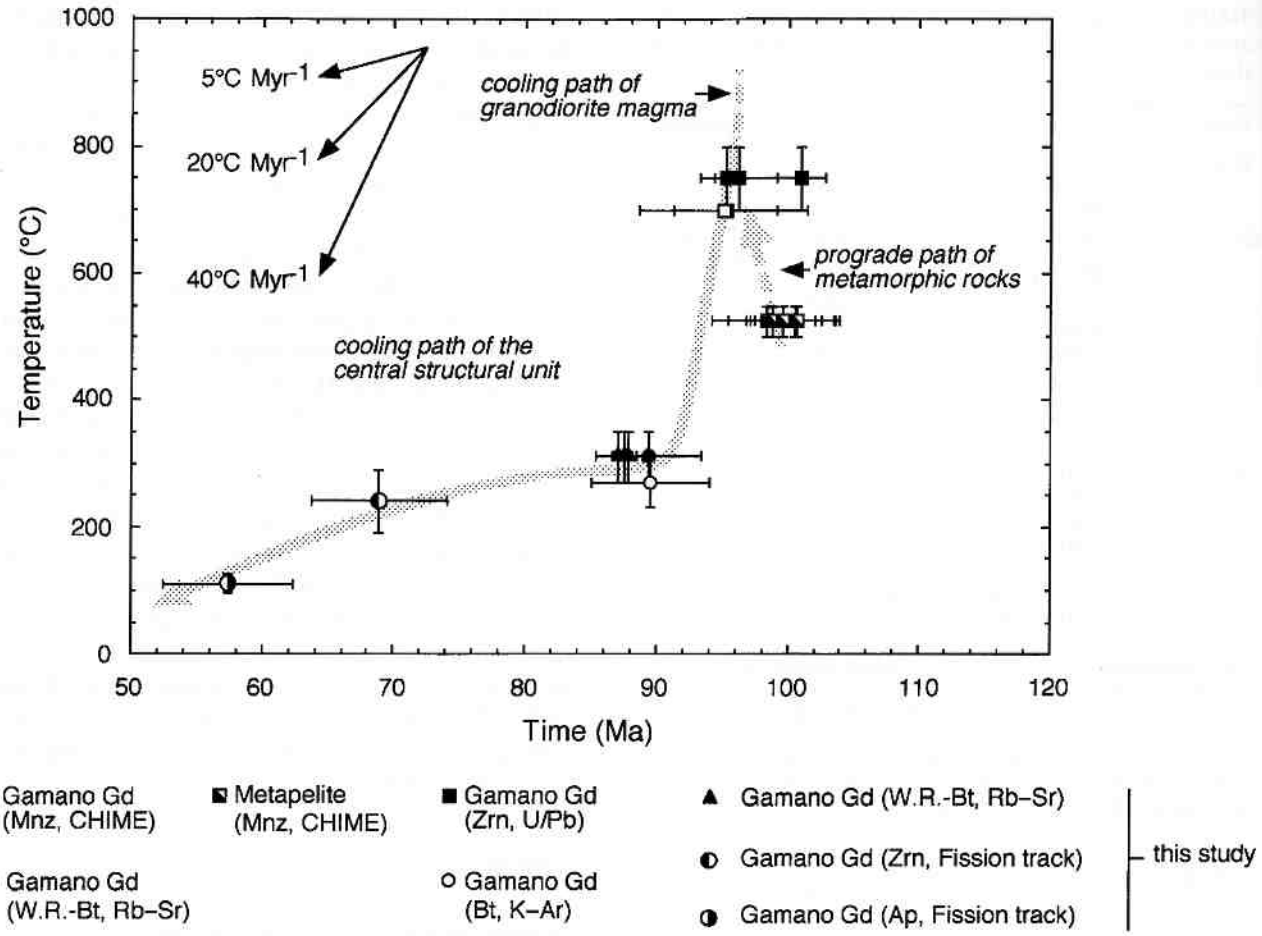

Fig. 7 Cooling history of the central unit of the Ryoke metamorphic belt in the Yanai district. In this figure, the range of age represented by the length of the bar reflects the two sigma error. Arrows indicate a possible temperature-time path (cooling history) of the rocks of the central structural unit. Two distinctive cooling stages can be recognized as: (1) a rapid cooling (>40°C/Myr) for a period (~7 Myr) soon after the thermal peak (*ca* 95 Ma) and (2) subsequently the slow cooling stage (approximately 5°C/Myr) after *ca* 88 Ma. Data sources for mineral ages; U–Pb zircon ages of the Gamano granodiorite: Herzig *et al.* (1998), SHRIMP zircon age of the Gamano granodiorite: Nakajima *et al.* (1993), CHIME monazite ages of the Gamano granodiorite and metapelites: Suzuki *et al.* (1994), Rb–Sr whole rock-biotite isochron age, recalculated based on $\lambda^{87}Rb = 1.42 \times 10^{-11}$/yr, of the Gamano granodiorite: Shigeno and Yamaguchi (1976), K–Ar biotite ages of the Gamano granodiorite: Higashimoto *et al.* (1983), and Rb–Sr whole-rock–mineral isochron ages and fission-track ages of zircon and apatite grains of the Gamano granodiorite: this study. CHIME, chemical Th–U-total Pb isochron method.

before the time of regional cooling to ~300 °C at approximately 88 Ma.

The central structural unit that includes the Gamano granodiorite was uplifted by low-angle thrusting and faulting to form the pile nappe structure of D2 and by D3 upright folds under an arc-normal compressional stress regime (see Fig. 2). In the granodiorite, the solid-state deformation structures are rarely observed, whereas long axes of euhedral-subhedral plagioclase and biotite grains are strongly aligned to form a distinct gneissose structure of D1 (Sakurai & Hara 1990; Okudaira 1996b). It follows that the gneissose structure was mainly formed by magmatic and/or submagmatic flow and was partly modified by high-temperature (high-T) ductile deformation of D2 and D3. Temperature estimation, using a two-feldspar geothermometry for myrmekite and K-feldspar grains (Stormer 1975; Stormer & Whitney 1977; Haselton *et al.* 1983), is of 510–560°C (plagioclase $X_{ab} = 0.66$, $X_{or} = 0.01$; orthoclase $X_{ab} = 0.13$, $X_{or} = 0.87$). This value is significantly lower than the solidus temperature of granodioritic rocks (approximately 750°C), and myrmekite was therefore formed by subsolidus deformation (Simpson & Wintsch 1989). Such a high-T deformation event took place before *ca* 88 Ma, because the estimated temperature is higher than the closure temperature of biotite for Rb–Sr system (310 ± 40°C). Therefore, uplift of the rocks

related to the high-T ductile deformation in the central unit took place at least before *ca* 88 Ma and the first cooling stage is related to the D2 and D3 deformation events. Furthermore, the formation of the D3 structures predated the intrusion of the Younger granitoids in the Yanai district. The CHIME monazite ages of the Younger granitoids fall in a range of 93–89 Ma (Suzuki *et al.* 1996; Suzuki & Adachi 1998). These ages indicate that the formation of D3-upright folds occurred at or before 93–89 Ma.

Exhumation velocity of the first cooling stage: constraints from numerical simulation

To estimate the velocity of the exhumation from data of the cooling rate, the assumption of which the temperatures of the rocks were equilibrated to the confining geotherm is necessary. However, the temperatures of the rocks in the central structural unit were not equilibrated to the geotherm, at least, for the initial period of the first cooling stage, because thermal perturbation caused by the intrusion of the granodiorite magma occurred.

To obtain an average exhumation velocity for the first rapid cooling stage, we evaluated a simple 1-D thermal model for the rocks of the central structural unit. The model used here modified the thermal model of Okudaira (1996b) which did not incorporate the exhumation process. The exhumation mechanism of the Ryoke metamorphic belt depended mainly on the uplift and erosion processes, because the crust became thickened by D2 and D3 deformation events under an arc-normal compression. Although outline of the model and procedure of the numerical simulation are described in the Appendix, some essentials of the model are described as follows. Boundary conditions of the model domain are constant temperature (0°C) at the Earth's surface and constant mantle heat flux at the bottom of the lithosphere. The thickness of the lithosphere before the intrusion of the granodiorite is assumed to be 30 km. As the mean geothermal gradient of an active continental margin or island arc is ~30°C/km (Sugimura & Uyeda 1973), the initial geotherm in the lithosphere is set to be ~30 °C/km and then mantle heat flux would be assumed to be 0.08 W/m^2. Depth of the sillimanite and garnet–cordierite zones can be estimated to be ~15 km (P = 0.4 GPa) and 20 km (P = 0.55 GPa), respectively and then a 4-km thick sheet of intrusion between 15.75 and 19.75 km in depth was assumed. We modeled the emplacement of the granodiorite magma as an instantaneous single intrusion. The instantaneous emplacement of pluton is assumed to simplify the model, because theoretical studies suggest that magmas rise quickly relative to their rate of cooling (Rothstein & Hoisch 1994). After the intrusion, thickness of the lithosphere instantaneously increases to 35 km (Fig. A-1a), and the lithosphere uplifts with the velocity v. Erosion rate of the Earth's surface is set to be equal to the uplift velocity, and then v is the exhumation rate. During the exhumation, the lithosphere becomes thinner and then the value of the geothermal gradient increases (Fig. A-1b). In this model, a relatively high initial intrusion temperature, 900°C, is assumed. The initial temperature of the granodiorite magma should have been much higher than approximately 800°C, because the temperatures of the garnet–cordierite zone attained to approximately 800°C (Okudaira 1996b; Ikeda 1998b) and source region of the magma was deeper than that of the garnet–cordierite zone. The Gamano granodiorite had fluid-like behavior at the time of its intrusion, because it shows many magmatic deformation structures. When the granitic magma has a crystallinity less than about 25%, fluid-like behavior occurs (Bergantz 1990). Therefore, the granodiorite magma had probably high melt fraction (> approximately 75%) during its intrusion. Assuming a linear relationship between the intrusion temperature and the melt fraction, the intrusion temperature of the granodiorite magma is 900°C, when the liquidus and solidus temperatures are set to be 950°C and 750°C, respectively.

Figure 8a shows temperature-time paths of the bottom of the granodiorite initially located at 19.5 km depth which is next to the country rock (array spacing = 500 m). In this figure, four cooling paths with exhumation velocities from 0 to 4 mm/yr are shown. As the temperature of the rocks of the central structural unit decreases to approximately 300°C during ~7 Myr, exhumation velocity of 2 mm/yr is suitable for the model. In this case, crust with a thickness of approximately 14 km is uplifted and eroded. Although the exhumation is assumed to have started at the same time with the granodiorite intrusion, there is no evidence that onset of the exhumation was simultaneous with the intrusion. To clarify the effect of time difference between the onset of the exhumation and the granodiorite intrusion, we simulated temperature-time relation so that timing of onset of the exhumation changes from 0 to 5 Myr after the intrusion. As shown in Fig. 8b, if the onset of the exhuma-

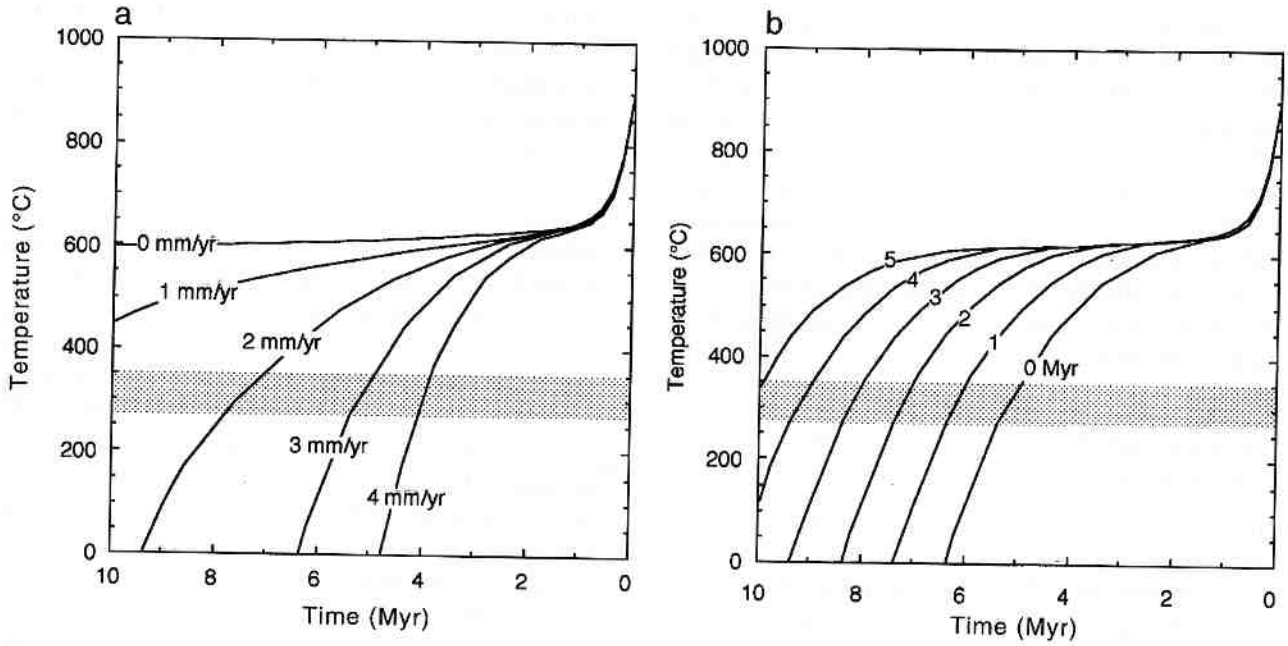

Fig. 8 Temperature-time paths at bottom of the granodiorite initially located at 19.5 km depth. Closure temperature for biotite in Rb–Sr system (310 ± 40 °C) is also drawn as stippled parts (▨). (a) Onset of the exhumation occurs at the same time of the granodiorite intrusion. Velocities of the exhumation are assumed to be from 0 to 4 mm/yr. (b) Onset of the exhumation is after the granodiorite intrusion by 0–5 Myr. The velocity is 3 mm/yr.

tion is 1–2 million years after the intrusion, exhumation velocity of 3 mm/yr is suitable for the model. Consequently the simulation suggests that the minimum velocity of the exhumation is approximately 2 mm/yr, and if there is a time difference between the onset of the exhumation and the granodiorite intrusion, the velocity is much higher than 2 mm/yr. This estimated velocity corresponds with the early stage denudation rate (1.5 mm/yr) in the western part of the Ryoke metamorphic belt suggested by Suzuki and Adachi (1998). Their estimation was based on the time-depth relations between the CHIME monazite ages and peak-*P* condition of the metapelites in the sillimanite zone, and the K–Ar biotite ages of the gneisses and granitoids, and its closure temperature in combination with a high geotherm of 80°C/km. These exhumation rates are within the range of the uplift/erosion rate for Phanerozoic orogenic belts such as the Alps and Himalayas (e.g. Clark & Jäger 1969; Hurford 1986; Wesnousky *et al.* 1999).

Exhumation velocity of the second slow cooling stage

As ductile deformation structures after D3 cannot be recognized, at least in the Yanai district, it is possible that the rocks of the central structural unit were statically uplifted after *ca* 88 Ma. For the second cooling stage, if the exhumation process was mainly uplift/erosion and the geothermal gradient was of 50–30°C/km, the exhumation velocity is 0.1–0.2 mm/yr. These values are smaller than the late-stage denudation rate (0.5 mm/yr) estimated by Suzuki and Adachi (1998). As their estimation was based on an indirect constraint from the deposition of the Upper Campanian to Maestrichtian Izumi Group on the high-grade gneiss and granitoid in western Shikoku, the exhumation velocity estimated here is more reliable than that of Suzuki and Adachi's estimation.

There is a difference in the exhumation velocity between the first and second cooling stages. One possibility is that uplift/erosion of mountain belts is fastest when the crust is at its maximum thickness, such as in the Himalayas, during the early stages of orogenesis. With time, as the crust thins and approaches isostatic equilibrium, uplift/erosion slows (e.g. Cosca *et al.* 1991). Another possibility is that the formation of the pile nappes and upright folds resulted in the crust becoming thick and uplift of the crust was enhanced. The second cooling stage was not accompanied by ductile

deformation, whereas during the first cooling stage an intense ductile deformation occurred. These two mechanisms possibly took place together in the Ryoke metamorphic belt in the Yanai district.

CONCLUSIONS

Four Rb–Sr whole-rock–mineral (biotite, plagioclase and K-feldspar) ages of the Gamano granodiorite in the Yanai district, south-west Japan, fall in a range of *ca* 89–87 Ma. The fission-track zircon and apatite ages are of 68.9 ± 2.6 Ma and 57.4 ± 2.5 Ma (1σ error), respectively. These newly obtained ages in combination with previously reported U–Pb and CHIME ages for the central structural unit, two distinctive cooling stages have been revealed: (i) a rapid cooling (>40°C/Myr) for a period of approximately 7 Myr soon after the thermal peak of the metamorphism (approximately 95 Ma); and (ii) the subsequent slow cooling stage (approximately 5°C/Myr) after *ca* 88 Ma. The first rapid cooling stage corresponds to thermal relaxation of the intruded granodiorite magma and its associated 'regional' low-pressure metamorphic rocks. It also corresponds to the uplift of the metamorphic complex by a displacement along low-angle normal and thrust faults which initiated soon after the intrusion. The later stage deformation formed large-scale upright folds resulting in further uplift of the rocks during the first stage. The average exhumation velocity of the stage is ≥2 mm/yr. During the second slow cooling stage, the rocks were statically exhumed with the rate of 0.1–0.2 mm/yr. The difference in the exhumation velocity between the first and second cooling stages resulted probably from the difference in the thickness of the crust and in the activity of the ductile deformation between the early and later stages of the orogenesis.

ACKNOWLEDGEMENTS

Three of the present authors (Okudaira, Hayasaka and Ohtomo) were research fellows at the Institute for Studies of Earth's Interior (ISEI), Okayama University in 1990. We thank H. Kagami for analytical advice on the Rb–Sr dating at the ISEI and I. Hara and T. Takeshita for many useful comments. Co-author (Himeno) would like to thank A.M. Grist, R. Mackay and M. Zentilli for their kind support in the Fission Track Research Laboratory at Dalhousie University. The paper benefited substantially from detailed reviews by M. Aoya, Y. Hiroi and K. Suzuki. S. Banno is thanked for the editorial handling of the manuscript.

REFERENCES

BERGANTZ G. W. 1990. Melt fraction diagrams: the link between chemical and transport models. *In* Nicholls J. & Russell J. K. (eds.) *Modern methods of igneous petrology: understanding magmatic processes. Reviews in Mineralogy* **24**, 240–57.

BROWN M. 1998. Unpairing metamorphic belts: P-T paths and a tectonic model for the Ryoke belt, southwest Japan. *Journal of Metamorphic Geology* **16**, 3–22.

CLARK S. P. J. R. & JÄGER E. 1969. Denudation rate in the Alps from geochronologic and heat flow data. *American Journal of Science* **267**, 1143–60.

COSCA M. A., SUTTER J. F. & ESSENE E. J. 1991. Cooling and inferred uplift/erosion history of the Grenville orogen, Ontario: constraints from $^{40}Ar/^{39}Ar$ thermochronology. *Tectonics* **10**, 959–77.

GALBRAITH R. F. 1981. On statistical models for fission track counts. *Mathematical Geology* **13**, 471–88.

GLEADOW A. J. W. 1981. Fission-track dating methods: What are the real alternatives? *Nuclear Tracks* **5**, 3–14.

GREEN P. F. 1981. A new look at statistics in the fission track dating. *Nuclear Tracks* **5**, 77–86.

GREEN P. F., DUDDY I. R., GLEADOW A. J. W., TINGATE P. R. & LASLETT G. M. 1986. Thermal annealing of fission tracks in apatite: 1. A qualitative description. *Chemical Geology* **59**, 237–53.

HANSON R. B. & BARTON M. D. 1989. Thermal development of low-pressure metamorphic belts: Results from two-dimensional numerical models. *Journal of Geophysical Research* **94** 10363–77.

HARA I., SAKURAI Y., OKUDAIRA T., HAYASAKA Y., OHTOMO Y. & SAKAKIBARA N. 1991. [Tectonics of the Ryoke belt.] *Excursion Guidebook, 98th Annual Meeting of the Geological Society of Japan.* Geological Society of Japan, Matsuyama pp. 1–20. (in Japanese).

HASELTON H. T., HOVIS G. L., HEMINGWAY B. S. & ROBIE R. A. 1983. Calorimetric investigation of the excess entropy of mixing in analbite-sanidine solid solution: lack of evidence for Na, K short-range order and implications for two-feldspar thermometry. *American Mineralogist* **68**, 398–413.

HERZIG C. T., KIMBROUGH D. L., TAINOSHO Y., KAGAMI H., IIZUMI S. & HAYASAKA Y. 1998. Late Cretaceous

U/Pb zircon ages and Precambrian crustal inheritance in Ryoke granitoids, Kinki and Yanai districts, Japan. *Geochemical Journal* **32**, 21–31.

HIGASHIMOTO S., NUREKI T., HARA I., TSUKUDA E. & NAKAJIMA T. 1983. Geology of the Iwakuni district. *Quadrangle series, scale 1 : 50 000.* Geological Survey of Japan, Tsukuba (in Japanese with English abstract).

HONMA H. & SAKAI H. 1975. Oxygen isotope study of metamorphic and granitic rocks of the Yanai district in the Ryoke belt, Japan. *Contributions to Mineralogy and Petrology* **52**, 107–20.

HURFORD A. J. 1986. Cooling and uplift patterns in the Lepontine Alps South Central Switzerland and an age of vertical movement on the Insubric fault line. *Contributions to Mineralogy and Petrology* **92**, 413–27.

HURFORD A. J. & GREEN P. F. 1983. The zeta age calibration of fission-track dating. *Isotope Geoscience* **1**, 285–317.

IKEDA T. 1991. Heterogeneous biotite from Ryoke metamorphic rocks in the Yanai district, southwest Japan. *Journal of the Geological Society of Japan* **97**, 537–47.

IKEDA T. 1998a. Progressive sequence reactions of the Ryoke metamorphism in the Yanai district, southwest Japan: the formation of cordierite. *Journal of Metamorphic Geology* **16**, 39–52.

IKEDA T. 1998b. Phase equilibria and the pressure-temperature path of the highest-grade Ryoke metamorphic rocks in the Yanai district, SW Japan. *Contributions to Mineralogy and Petrology* **132**, 321–35.

JÄEGER J. C. 1964. Thermal effects of intrusions. *Reviews of Geophysics* **2**, 44–54.

JÄGER E. 1979. Introduction to Geochronology. *In* Jäger E. & Hunziker J. C. (eds.) *Lectures in isotope geology*, pp. 1–12. Springer, New York.

KAGAMI H., IWATA M., SANO S. & HONMA H. 1987. Sr and Nd isotopic compositions and Rb Sr, Sm and Nd concentrations of standard samples. *Technical Report of Institute for Studies of the Earth's Interior, Okayama University, Series B* **4**, 1–16.

KAGAMI H., YOKOSE H. & HONMA H. 1989. $^{87}Sr/^{86}Sr$ and $^{143}Nd/^{144}Nd$ ratios of GSJ rock reference samples; JB-1a, JA-1 and JG-1a. *Geochemical Journal* **23**, 209–14.

KAWANO Y. 1994. Calculation program for isochron ages of Rb-Sr and Sm-Nd systems using personal computer. *Geoinformatics* **5**, 13–9 (in Japanese with English abstract).

KOJIMA G. & OKAMURA Y. 1968. On the Kitaoshima granite gneiss complex. *Journal of Science of the Hiroshima University, Series C* **5**, 295–306.

KUTSUKAKE T. 1993. An initial continental margin plutonism—Cretaceous Older Ryoke granitoids, southwest Japan. *Geological Magazine* **130**, 15–28.

MCDOUGALL I. & HARRISON T. M. 1988. *Geochronology and thermochronology by the $^{40}Ar/^{39}Ar$ method.* Oxford, New York.

MIYASHIRO A. 1994. *Metamorphic petrology.* UCL Press, London.

NAKAJIMA T. 1994. The Ryoke plutonometamorphic belt: crustal section of the Cretaceous Eurasian continental margin. *Lithos* **33**, 51–66.

NAKAJIMA T., WILLIAMS I. S. & WATANABE T. 1993. [SHRIMP U-Pb ages of the Ryoke and San-yo granitoids in Southwest Japan.] *Abstract with Programs, 100th Annual Meeting of the Geological Society of Japan*, 584 (in Japanese). Geological Society of Japan, Matsuyama.

NISHIMURA S. & MOGI T. 1986. The interpretation of discordant ages of some granitic bodies. *Journal of the Geothermal Research Society of Japan* **8**, 145–64.

NUREKI T., ENAMI M., SHIOTA T. & SHIBATA T. 1992. Paired metamorphic belts: Ryoke and Sanbagawa. *29th International Geological Congress field trip guide book* **5**, 103–32.

OHTOMO Y. 1993. Origin of the Median Tectonic Line. *Journal of Science of the Hiroshima University, Series C* **9**, 611–69.

OKANO O. & HONMA H. 1983. Sr isotope ratio of the Ryoke and Hiroshima granitic rocks in the Yanai district. *Magma* **67**, 123–8. (in Japanese).

OKUDAIRA T. 1996a. Temperature-time path for the low-pressure Ryoke metamorphism, Japan, based on chemical zoning in garnet. *Journal of Metamorphic Geology* **14**, 427–40.

OKUDAIRA T. 1996b. Thermal evolution of the Ryoke metamorphic belt, southwestern Japan: Tectonic and numerical modeling. *The Island Arc* **5**, 373–85.

OKUDAIRA T. 1996c. Low-pressure metamorphism in the Ryoke metamorphic belt in the Yanai district, southwest Japan. *Journal of Science of the Hiroshima University, Series C* **10**, 509–18.

OKUDAIRA T., HARA I., SAKURAI Y. & HAYASAKA Y. 1993. Tectono-metamorphic processes of the Ryoke belt in the Iwakuni-Yanai district, southwest Japan. *Memoirs of the Geological Society of Japan* **42**, 91–120.

O'SULLIVAN P. B. & PARRISH R. R. 1995. The importance of apatite composition and single-grain ages when interpreting fission track data from plutonic rocks: a case study from the Coast Ranges, British Columbia. *Earth and Planetary Science Letters* **132**, 213–24.

PEACOCK S. M. 1989. Numerical constrains on rates of metamorphism, fluid production, and fluid flux during regional metamorphism. *Geological Society of America Bulletin* **101**, 476–86.

PEACOCK S. M. 1991. Thermal modeling of metamorphic pressure—temperature—time paths: A forward approach. *In* Spear F. S. & Peacock S. M. (eds.) *Metamorphic pressure-temperature-time paths, Short Course in Geology. American Geophysical Union* **7**, 57–102.

ROTHSTEIN D. A. & HOISCH T. D. 1994. Multiple intrusions and low-pressure metamorphism in the central Old Woman Mountains, south-eastern California: constraints from thermal modelling. *Journal of Metamorphic Geology* **12**, 723–34.

RYOKE RESEARCH GROUP. 1972. The mutual relations of the granitic rocks of the Ryoke metamorphic belt in central Japan. *Earth Science* **26**, 205–16 (in Japanese with English abstract).

SAKURAI Y. & HARA I. 1988. Emplacement, deformation and mineral textures of the Yagyu granite, central Japan. *Extended Abstracts, Fifth International Synposium on Tin/Tungsten Granites in Southeast Asia and the Western Pacific*, Shimane University, Matsue, pp. 153–7.

SAKURAI Y. & HARA I. 1990. [Deformation styles and tectonics of granitic rocks of the Ryoke belt (I) Deformation styles of plagioclase.] *Earth Monthly* **12**, 457–61 (in Japanese).

SCHMIDT M. W. 1992. Amphibole composition in tonalite as a function of pressure: an experimental calibration of the Al-in-hornblende barometer. *Contributions to Mineralogy and Petrology* **110**, 304–10.

SHIGENO H. & YAMAGUCHI M. 1976. A Rb-Sr isotopic study of metamorphism and plutonism in the Ryoke belt, Yanai district. *Journal of the Geological Society of Japan* **82**, 687–98 (in Japanese with English abstract).

SIMPSON C. & WINTSCH R. P. 1989. Evidence for deformation-induced K-feldspar replacement by myrmekite. *Journal of Metamorphic Geology* **7**, 261–75.

SMITH H. A. & BARREIRO B. 1990. Monazite U-Pb dating of staurolite grade metamorphism in pelitic schist. *Contributions to Mineralogy and Petrology* **105**, 602–15.

SPEAR F. S. 1993. *Metamorphic phase equilibria and pressure-temperature-time paths.* Mineralogical Society of America, Washington D.C.

STEIGER R. H. & JÄGER E. 1977. Subcommission on geochronology: Convection on the use of decay constants in geo- and cosmochronology. *Earth and Planetary Science Letters* **36**, 359–62.

STORMER J. C. 1975. A practical two-feldspar geothermometer. *American Mineralogist* **60**, 667–74.

STORMER J. C. & WHITNEY J. A. 1977. Two-feldspar geothermometry in granulite facies metamorphic rocks. *Contributions to Mineralogy and Petrology* **65**, 123–33.

SUGIMURA A. & UYEDA S. 1973. *Island arcs, Japan, and its environs.* Elsevier, Amsterdam.

SUZUKI K. & ADACHI M. 1998. Denudation history of the high T/P Ryoke metamorphic belt, southwest Japan: constraints from CHIME monazite ages of gneisses and granitoids. *Journal of Metamorphic Geology* **16**, 23–38.

SUZUKI K., ADACHI M. & KAJIZUKA I. 1994. Electron microprobe observations of Pb diffusion in metamorphosed detrital monazites. *Earth and Planetary Science Letters* **128**, 391–405.

SUZUKI K., ADACHI M. & NUREKI T. 1996. CHIME age dating of monazites from metamorphic rocks and granitic rocks of the Ryoke belt in the Iwakuni area, Southwest Japan. *The Island Arc* **5**, 43–55.

TAGAMI T., GALBRAITH R. F., YAMADA R. & LASLETT G. M. 1999. Revised annealing kinetics of fission tracks in zircon and geological implications. *In* Van Den Haute P. & De Corte F. (eds.) *Advances in fission-track geochronology*, pp. 99–112. Kluwer Academic Publishers, Dordrecht.

TAGAMI T., LAL N., SORKHABI R. & NISHIMURA S. 1988. Fission track thermochronological analysis of the Ryoke belt and the Median Tectonic Line, Southwest Japan. *Journal of Geophysical Research* **93**, 13705–25.

TURCOTTE D. L. & SCHUBERT G. 1982. *Geodynamics.* John Wiley, New York.

WELLS P. R. A. 1980. Thermal models for the magmatic accretion and subsequent metamorphism of continental crust. *Earth and Planetary Science Letters* **46**, 253–65.

WESNOUSKY S. G., SENTHIL KUMAR MOHINDRA R. & THAKUR V. C. 1999. Uplift and convergence along the Himalayan Frontal Thrust of India. *Tectonics* **18**, 967–76.

YORK D. 1966. Least-squares fitting of a straight line. *Canadian Journal of Physics* **44**, 1079–86.

YUHARA M. & KAGAMI H. 1995. Cooling history of the Katsuma quartz diorite in the Ina district of the Ryoke belt, Southwest Japan Arc. *Journal of the Geological Society of Japan* **101**, 434–42 (in Japanese with English abstract).

APPENDIX

PROCEDURE OF THE NUMERICAL SIMULATION

One-dimensional heat transfer equation can be written as

$$\frac{\partial T}{\partial t} = \frac{K}{\rho_m C_m}\frac{\partial^2 T}{\partial z^2} - \mathbf{V}\cdot\frac{\partial T}{\partial z} + \frac{A}{\rho_m C_m} \qquad \text{(A-1)}$$

where ρ_m = density of rock (2750 kg/m^3); C_m = specific heat of rock (880 J/kg per K); T = temperature (K); t = time (s); K = thermal conductivity (2.8 W/m per K); z = vertical coordinate (m) measured from the earth's surface; $\mathbf{v}$ = vertical exhumation velocity (m/s); and A is the heat production of radioactive elements (W/m^3). Equation (A-1) was solved numerically using an explicit finite-difference method with a 500 m array spacing (Δz) and a 3.15×10^9 s time step (Δt).

Production of heat during the crystallizing magma, that is, latent heat, and consumption of heat by the

endothermic reactions are modeled in the simulation. In this section, only basic procedure is described (for further details see Okudaira 1996b). The production and consumption of heat were incorporated into the numerical model using an effective heat capacity, C^*, and an effective thermal diffusivity, κ^*, for rocks undergoing the reactions (Jäeger 1964; Hanson & Barton 1989; Peacock 1989). The effective thermal diffusivity is then calculated from

$$\kappa^* = \frac{K}{\rho_m C^*}. \qquad \text{(A-2)}$$

Following Wells (1980) and Hanson and Barton (1989), we have used the crystallization intervals of 950 and 750°C for the initial intrusion temperature of 900°C for granodioritic composition and taken the value of 3.35×10^5 J kg^{-1} for enthalpy of crystallizing magma.

Radiogenic heat production, the third term on the right side of Equation (A-1), of elements to decay decreases exponentially with depth according to the relation (Turcotte & Schubert 1982):

$$A = A_0 e^{-z/h_r} \qquad \text{(A-3)}$$

where A_0 and h are the surface radiogenic heat production (2.60×10^{-6} W/m^3) and the characteristic length scale (10 km), respectively. In contrast, for the magma, the heat production from the decay of radioactive elements A is represented by that of the magma A_g (2.64×10^{-6} W/m^3).

The initial continental geotherm immediately before the intrusion of magma is calculated from Turcotte and Schubert (1982):

$$T_i = T_s + \frac{q_m z}{K} + \frac{A_0 h r^2}{K}(1 - e^{-z/h_r}) \qquad \text{(A-4)}$$

where T_i, T_s and q_m are the initial temperature of the rock, the surface temperature and the mantle heat flux, respectively. In this study, the boundary conditions are constant temperature (0°C) at $z = 0$ and constant mantle heat flux, q_m, at the bottom of the lithosphere. The thickness of the lithosphere before the intrusion of the granodiorite is assumed to be 30 km. The initial geotherm in the lithosphere is set to be approximately 30°C/km and then q_m would be assumed to be 0.08 W/m^2.

According to the relation $z = P$ (in Pa)/$\rho_m \cdot g$, depth of the sillimanite and garnet–cordierite zones can be esti-

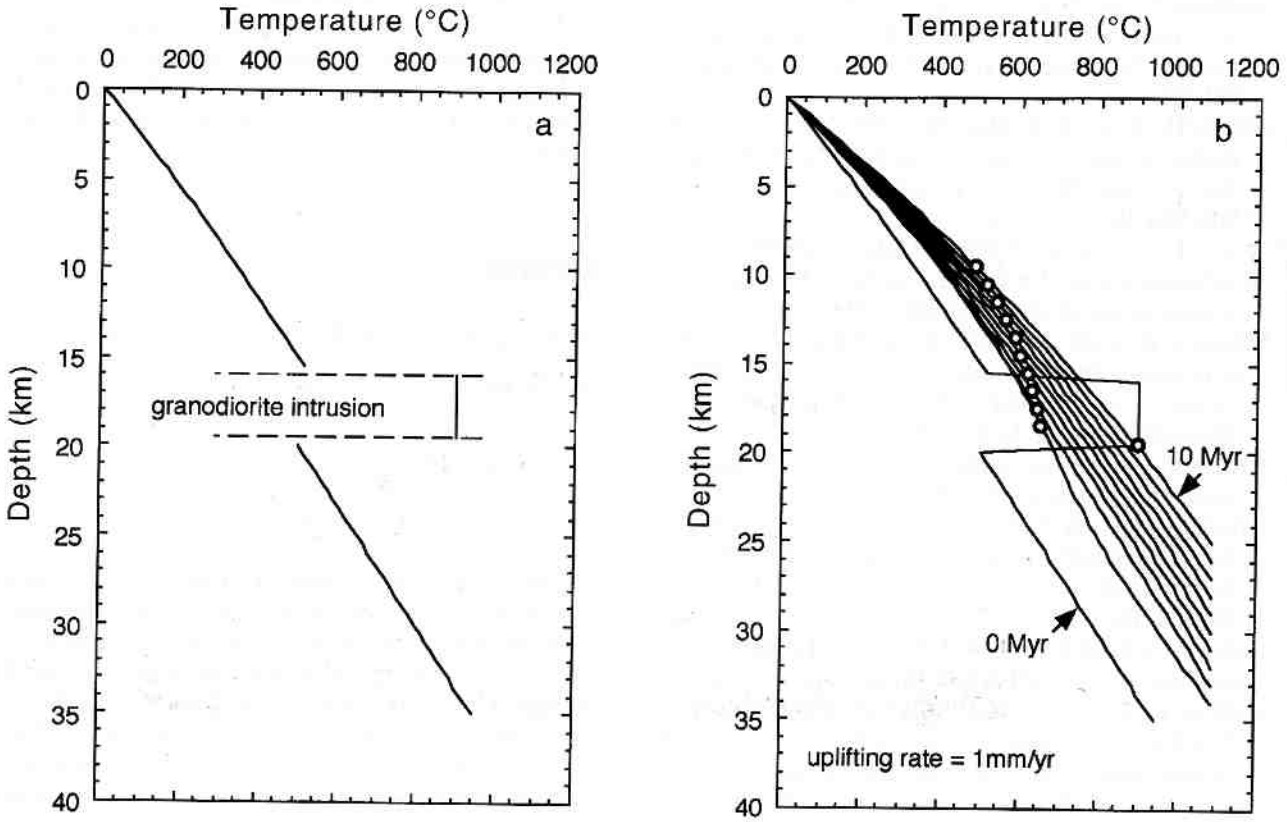

Fig. A-1 (a) Initial condition of the model. (b) Temperature-depth curves (v = 1 mm/yr) showing thermal evolution of the lithosphere, from 0 to 10 Myr (1 Myr intervals). Circles represent changing temperature of the rock, initially located 19.5 km depth, along with its exhumation, from 0 to 10 Myr (1 Myr intervals). See Appendix for explanation.

mated to be approximately 15 km ($P = 0.4$ GPa) and 20 km ($P = 0.55$ GPa), respectively, and then a 4-km thick sheet of intrusion between 15.75 and 19.75 km in depth was assumed. We modeled the emplacement of the granodiorite magma as an instantaneous single intrusion. After the intrusion, thickness of the lithosphere instantaneously inflates to 35 km (Fig.A-1a), and the lithosphere uplifts with the velocity v. Erosion rate of the Earth's surface is set to be equal to the uplift velocity, and then v is the exhumation rate. During the uplift, the lithosphere becomes thinner and the value of the geothermal gradient increases (Fig. A-1b).